ACS OMEGA

Open Access

http://pubs.acs.org/journal/acsodf

Article

Reaction Mechanism of Nitrogen-Containing Heterocyclic Compounds Affecting Coal Spontaneous Combustion

Mengmeng Zhang, Zhilin Xi,* Zhensen Gong, and Yubo Dong

Cite This: *ACS Omega* 2023, 8, 35295−35306

Read Online

ACCESS | Metrics & More | Article Recommendations

ABSTRACT: To uncover the reaction mechanism of nitrogen-containing heterocyclic compounds affecting coal self-heating, quantum chemical calculations and X-ray photoelectron spectroscopy (XPS) experiments were applied to elucidate the reaction pathways and thermodynamic characteristics of pyrrole, pyridine, indole, quinoline, and carbazole. Results show that in pyrrole, pyridine, indole, quinoline, and carbazole, the reaction with O_2 captures the H atom and leads to the formation of ·OOH and pyrrolyl, pyridinyl, indolyl, quinolinyl, and carbazolyl radicals, respectively. The activation energies are 118.15, 86.642, 34.132, 21.004, and 47.259 kJ/mol, respectively. ROO· formed by spontaneous adsorption of O_2 by nitrogen-containing radicals undergoes self-reaction, and the O−O bond is broken and dehydrogenated to generate ·OH. Subsequently, at room temperature, ·OH reacts with pyrrole, pyridine, indole, quinoline, and carbazole, resulting in the formation of H_2O and pyrrolyl, pyridinyl, indolyl, quinolinyl, and carbazolyl radicals, respectively, thereby forming a cyclic chain reaction. The XPS analysis yielded the following findings: (i) when the temperature rises to 70 °C, the N-5 and N-6 content decrease, which is attributed to the activation energy; (ii) when the temperature reaches 200 °C, the N-5 content decreases, which can be attributed to the activation energy required for the oxidation of pyrrole (118.5 kJ/mol).

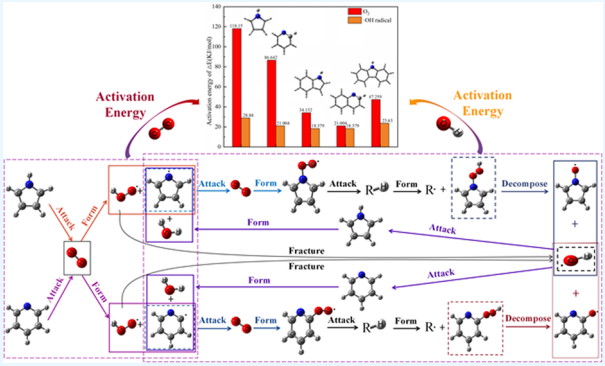

1. INTRODUCTION

Coal, as a fundamental fuel for industrial and civilian applications, holds significant importance as an energy source for humans.[1] In 2022, China recorded a production of 46.6 tons of raw coal, thereby making a notable increase of 9.2% compared with that of the previous year. Coal consumption experienced an increase of 4.3%, representing 56.2% of the total energy consumption. This figure reflects an increase of 0.3 percentage points compared with the previous year.[2] However, low-rank coal is prone to exothermic slow oxidation, which, along with the heat accumulation, can lead to the breakage of the coal molecular bond to produce combustible gases, thus causing mine fires. The low-temperature oxidation of coal has a significant effect on the structure and elemental composition of the coal body. This process leads to a reduction in the calorific value of coal and the release of substantial quantities of greenhouse gases (CO_2, CH_4), toxic gases (CO, H_2S, NOx, N_2O, and SO_2), and certain harmful trace elements (As, F, Hg, and Se). Consequently, this oxidation-induced transformation contributes to environmental pollution.[3] Among them, the greenhouse gases released by coal spontaneous combustion (CSC) account for 0.10−0.22% of CO_2 emissions from fossil fuels.[4] Notably, the CSC is recognized as one of the main sources of carbon emissions in China. However, CSC, accounting for 91.6% of accidents involving more than 100 people,[5] is the main ignition source of gas explosion disasters.[6]

Scholars have conducted extensive research on the mechanisms of CSC and have proposed the doctrines of pyrite action, phenol-based action, free radical action, and coal−oxygen complex action to explain them.[7] Free radical theory is generally accepted and posits that under specific conditions, including external forces, heat sources, and UV light irradiation, the covalent bonds within the organic macromolecule chains of coal can break, resulting in the generation of a significant number of free radicals, which will further oxidize and undergo chain reactions, thus inducing CSC.[8] Zhou et al.[9] used electron spin resonance to assess the concentration of free radicals in the coal body under different O_2 concentrations; their investigation revealed that a large number of radicals were generated during the chain reaction. Xu et al.[10] studied the reaction of free radicals and oxygen-

Received: July 15, 2023
Accepted: September 4, 2023
Published: September 18, 2023

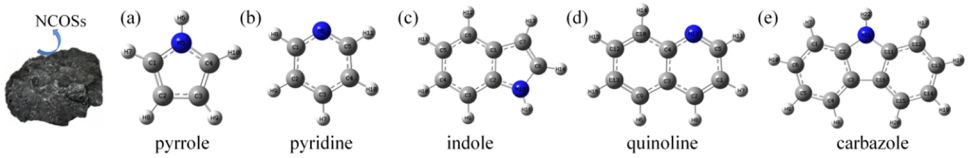

Figure 1. Optimized molecular models: (a) pyrrole; (b) pyridine; (c) indole; (d) quinoline; (e) carbazole.

containing functional groups during the low-temperature oxidation of different grades of coal. Their investigation obtained the following findings: when the temperature was higher than 90 °C, types and concentrations of free radicals increased rapidly, the chain reaction was rapid, and the movement of free radicals was intensified, thereby suggesting an increase in coal oxidation activity. Zhou et al.[11] showed that different oxygen concentrations had varying effects on the reactivity of coal groups. Furthermore, when the oxygen concentration was >9 %, −C═O and −COOH were more active in the oxidation process, which caused the occurrence of ring−chain reactions. Xin et al.[12] demonstrated that the presence of lone pairs of electrons in the molecular structure of the coal surface enhanced the oxidation reaction of coal. Chen et al.[13] showed that the alkane radical generated hydrogen peroxide radicals and released a significant amount of heat during CSC. Xi et al.[14] concluded that the primary pathways of ·OH formation in coal bodies involved ·OOH and ROO· direct decomposition. Furthermore, they elucidated the reaction pathway of ·OH during low-temperature oxidation, emphasizing the pivotal role of ·OH in the free radical chain reaction. Qi et al.[15] used quantum chemistry to study the reaction pathway and thermodynamic characteristics of carboxyl groups in the self-heating process of coal. Xi et al.[16] discussed the reaction mechanisms of organosulfur model compounds in CSC process and found that the oxidation of 2-methylthiophene accelerated the autogenous chain reaction of coal.

The nitrogen content in coal is relatively scarce and exists in complex forms. Some scholars have also directed their attention to examining the impact of nitrogen on the CSC process. Cao et al.[17] identified 21 nitrogen-containing heterocyclic compounds (NCOSs) in Pocahontas No. 3 coal, and nitrogen was mainly found in pyrrole, pyridine, indole, quinoline, and carbazole, etc. Ikeda et al.[18] suggested that the o-pyridinyl radical generated by the interaction of oxygen with the broken C−H bond in pyridine plays a crucial role in coal oxidation. Zheng et al.[19] concluded that in the oxidation reactions of N-containing molecular structures in coal bodies, O_2 abstracts H from the N−H bond in pyrrole. Laskin and Lifshitz[20] explored the reaction mechanism of indole using a combination of molecular dynamics and experimental methods. They found that indole undergoes intramolecular hydrogen transfer to eventually generate HCN. Wu et al.[21] proposed a new kinetic model of pyrrole (including 196 species and 2939 reactions) and concluded that the main nitrogen carrier of pyrrole pyrolysis products was trinitromethane, and the important intermediates included $C_3H_2N_2$ and $C_4H_4N_2$. Wang et al.[22] concluded that at low temperatures, pyridine and pyrrole were oxidized to form HCN and CO; at high temperatures of 800 °C, pyridine and pyrrole were oxidized to produce N_2 and N_2O. Luo et al.[23] found that carbon dioxide inhibited the spontaneous combustion of pyrrole by modeling pyrrole oxidation. Mai et al.[24] explored the potential energy surface characteristics of pyrrole oxidation induced by ·OH at the M06-2X/aug-cc-pVTZ theoretical level. Wu et al.[25] found that among various H-containing radicals, the hydroxyl radical contributed the highest absorption of nitrogen-containing heterocyclic groups. Yamamoto et al.[26] studied the decomposition reaction mechanism of pyrrole and found that pyrrole and pyridine can undergo interconversion and engage in ring cleavage, pyrolysis, and oxidation reactions to produce HCN.

Scholars have conducted extensive research on the pyrolysis of N-containing molecular structures and the conversion of H atoms in coal. However, microscopic-level analyses of the reaction pathways and thermal properties of nitrogen-containing heterocyclic groups in the context of CSC interaction are still lacking. Therefore, this paper aims to provide a comprehensive study of the reaction mechanism of NCOSs during coal oxidation. Through a combination of quantum chemical numerical calculations and experiments, our research seeks to shed light on the essential causes of CSC triggered by nitrogen-containing groups, which is of great significance to enriching the principles of CSC.

2. CALCULATION DETAILS AND EXPERIMENTAL SECTION

2.1. Calculation Methods. The nitrogen present in the coal structures is mainly found in the form of organic aromatic heterocycles. Among them, pyrrole with a nitrogenous five-membered ring and pyridine with a nitrogenous six-membered ring exhibit the simplest structures and are commonly used as model compounds for studying the structures of nitrogen-containing molecules.[27,28] However, pyrrole and pyridine do not exist independently in coal bodies and are often combined with aromatic rings to form carbazole, indole, and quinoline structures.[29−31] Therefore, in this paper, pyrrole, pyridine, indole, quinoline, and carbazole were examined to reveal the effects of nitrogen-containing molecular structures on CSC. The optimized model structure is shown in Figure 1.

The molecular structure was modeled using GaussView and calculated based on the DFT framework of the Gaussian 09. The molecular structure was optimized using the B3LYP function and 6-31G(d,p) basis group. The natural bond orbital (NBO) analysis method was used based on the optimized molecular conformations of the obtained complexes. The results show the bonding levels of each chemical bond in the molecule and the active site can be determined accurately. TS was selected to calculate the initial transition state, and an intrinsic reaction coordinate analysis was performed to determine whether reactants and products had only one imaginary frequency to verify the correctness of the transition state. The enthalpy change (ΔH) and activation energy (ΔE) of the reaction equation were extracted using Shermo software, and the electrostatic potential (ESP) of the molecular surface of coal (electron density = 0.02 au) was analyzed using Multiwfn 3.7 software, combined with the VMD1.9.4 program (Visual Molecular Dynamics) to analyze ESP isosurface map visualization results. The reaction rate constants were

https://doi.org/10.1021/acsomega.3c05088
ACS Omega 2023, 8, 35295−35306

Table 1. Ultimate and Proximate Analysis of Coal Samples[a]

species	proximate analysis (%)				ultimate analysis (%, daf)				
	Mad	Aad	Vad	FCad	C	H	O	N	S
HM	11.04	8.41	41.25	39.3	68.94	5.63	22.79	2.13	0.51
CY	7.84	6.82	37.14	48.2	75.43	4.89	18.58	0.98	0.12
FM	10.64	5.48	34.37	49.51	76.28	4.07	17.82	1.45	0.38
JM	1.14	22.44	21.32	55.1	80.2	4.05	14.33	1.21	0.21
WY	1.47	12.38	9.87	76.28	89.24	2.82	6.6	1.06	0.28

[a]Mad: moisture; Aad: ash; Vad: volatile; FCad: fixed carbon. ad- air-dry basis; daf- dry ash-free basis.

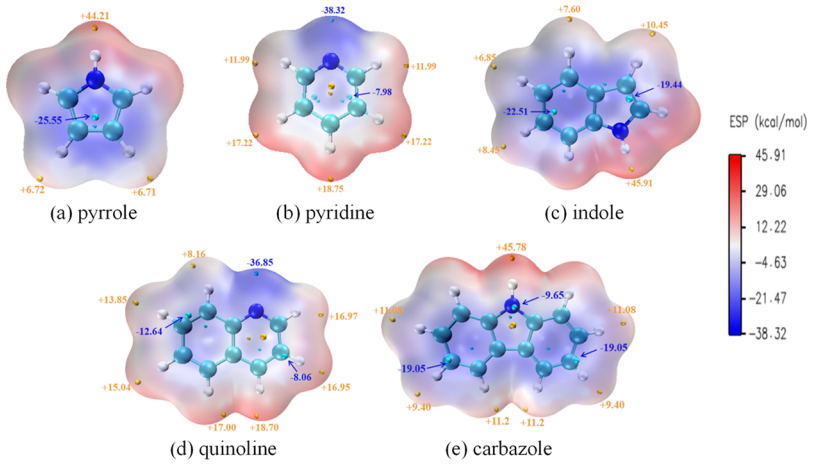

Figure 2. Molecular ESP of NCOSs: (a) pyrrole; (b) pyridine; (c) indole; (d) quinoline; (e) carbazole. (represents the point of maximum ESP, represents the point of minimum ESP).

calculated using TST theory, which assumes that the reactants are in thermodynamic equilibrium because of the rapid energy exchange with the environment and that all reactants in the transition state can be converted into products. It is calculated as follows:

$$K^{\mathrm{TST}} = \sigma \frac{k_{\mathrm{B}}T}{h}\left(\frac{RT}{P_0}\right)^{\Delta n} \mathrm{e}^{-\Delta G^{0,\neq}/(k_{\mathrm{B}}T)} \quad (1)$$

where σ = 1 is the degeneracy of the reaction path; k_{B} = 1.381e^{-23} J/K is Boltzmann's constant; T is the thermodynamic temperature, K; h = 6.626 × 10^{-34} J s is Planck's constant; R = 8.314 J/(mol K) is the universal constant; Δn = 1 is the bimolecular reaction; P_0 = 101.325 kPa is the pressure in the standard state; $\Delta G, \neq$ is the ΔE of the standard state, kJ/mol.

2.2. Experiments. In this paper, five coals with different degrees of coalification, namely, Shaanxi Lignite (HM), Shanxi Datong Coking coal (JM), Tangshan Fat coal (FM), Shanxi Datong Long-flame coal (CY), and Shanxi Hunyuan Anthracite (WY) were used. Under the protection of nitrogen, the fresh coal samples were ground and screened to produce a coal powder with a particle size of less than 0.048 mm for the experiments. The collected coal samples were dried under vacuum at 30, 70, and 200 °C for 48 h to remove a considerable amount of surface moisture. The results of ultimate and proximate analyses of the coal samples are listed in Table 1.

Narrow spectral scans of N 1s in HM, JM, and WY were performed using X-ray photoelectron spectroscopy (XPS, Thermo Fisher Scientific ESCALAB 250Xi). The XPS instrument parameters were set as follows: full-spectrum scan range of 0−1350 eV; broad-spectrum pass energy of 100 eV and scan step of 1 eV; narrow spectral region pass energy of 30 eV, and scan step of 0.1 eV. The binding energy of the C 1s peak was set to 284.8 eV. In this paper, peak fitting curve analysis of N 1s was performed using XPS PEAK 4.1. The surface composition (in %) was determined by considering the detected N 1s peak area.

3. RESULTS AND DISCUSSION

3.1. Active Site Analysis. The van der Waals surface ESP plays a crucial role in predicting intermolecular interactions.[32,33] In general, the ESP of C and H atoms in coal molecules is red, indicating a positive charge and their susceptibility to nucleophilic reactions. The ESP of the O atomic region is blue, indicating a negative charge and its propensity for electrophilic reactions. Figure 2 shows the molecular ESP of pyrrole, pyridine, indole, quinoline, and carbazole. Among them, the N−H bonds in pyrrole, carbazole, and indole, as well as the C−H bonds around pyridine and quinoline, are positively charged, indicating more susceptibility to nucleophilic reactions. The ESP analysis of pyrrole yielded a minimum value of −25.55 kcal/mol at the middle position of the group and a maximum value of 44.21 kcal/mol at the position of the H atom in the N−H bond. Therefore, the N−H bond on pyrrole is the active site, as shown in Figure 2a. The maximum and minimum points of indole and carbazole are located near the N−H bond, indicating that the bond is most likely to be the reactive site for oxygen capture of H atoms, as shown in Figure 2c,e, respectively. The smaller the ESP values of a site, the stronger its ability to attract electrophilic reagents and the more likely it is to be a reactive site. The active sites of pyridine and quinoline are in the C−H bond adjacent to the N

https://doi.org/10.1021/acsomega.3c05088
ACS Omega 2023, 8, 35295−35306

Table 2. NBO Analysis of NCOSs

reactant	occupancy	bond orbital	coefficients	hybrids
pyrrole	1.99163	N5−H6	(72.16%)0.8495*N5	s(29.02%),p(70.96%)
			(27.84%)0.5276*H6	s(99.90%),p(0.10%)
carbazole	1.98990	N21−H22	(72.30%)0.8503*N21	s(29.38%),p(70.60%)
			(27.70%)0.5263*H22	s(99.90%),p(0.10%)
indole	1.96637	N15−H16	(75.74%)0.8703*N15	s(36.72%),p(63.23%)
			(24.26%)0.4925*H16	s(99.86%),p(0.14%)
pyridine	1.98323	C5−H11	(61.68%)0.7854*C5	s(30.57%),p(69.38%)
			(38.32%)0.6190*H11	s(99.95%),p(0.05%)
quinoline	1.98241	C5−H11	(61.64%)0.7851*C5	s(30.32%),p(69.63%)
			(38.36%)0.6194*H11	s(99.95%),p(0.05%)

atom, and the minimum values in the ESP values are −38.32 and −36.85 kcal/mol, respectively, as shown in Figure 2b,d. The ESP distribution on the vdW surface is not uniform because of the different numbers of π-electrons on the atoms, and the small fraction of the vdW surfaces have large negative ESP values (i.e., < − 30 kcal/mol), which are mainly attributed to the N atom in pyridine and quinoline. The vdW surfaces of pyrrole, indole, and carbazole have higher ESP values of 44.21, 45.91, and 45.78 kcal/mol, respectively, mainly on the H atom attached to the N−H bond.

The results of ESP and NBO analyses can accurately determine the active sites of NCOSs because electrophilic attacks involve the formation or destruction of covalent bonds. Table 2 shows the analysis results of NBO and the following conclusions: N5−H6, C5−H11, N15−H16, N21−H22, and C5−H11 bonds of pyrrole, pyridine, indole, carbazole, and quinoline have the highest charge densities at 72.16, 61.68, 75.74, 72.30, and 61.64%, respectively. It has the strongest reactivity, which is consistent with the results of the ESP analysis.

3.2. Oxidation Pathway of NCOSs. *3.2.1. Mechanism of the Reaction of Pyrrole and Oxygen.*

Pyrrole is a five-membered heterocyclic structure with a multi-π electron system that is susceptible to electrophilic substitution reactions.[34] The oxidation reaction of pyrrole occurs mainly at the N−H bond, as shown in eq 2. The larger

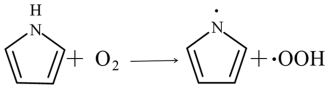

the Mayer bond order, the more stable and less likely it is to break; the smaller the bond order, the less stable and more likely it is to break the bond between atoms.[35] Figure 3 shows the energy barrier diagram of pyrrole oxidation and the Mayer bond order variation of N5−H6, H6−O11, and O11−O12 bonds. In the process of the O_2 extraction of the H atom in the N5−H6 structure, the bond order between N5 and H6 weakened and tended to break, and the bond order between H6 and O11 increased, whereas the bond order between O11 and O12 weakened, thereby promoting the formation of an unstable nitrogen-containing intermediate pyrrolyl radical and ·OOH. The reaction process overcomes an energy barrier of 118.15 kJ/mol and absorbs 144.4 kJ/mol of heat. The pyrrolyl radical generated by the oxidation of pyrrole is extremely unstable and is easily attacked again by O_2. The oxidation reaction occurs to generate pyrrolyl peroxy radical intermediates, as shown in eq 3. This process is a chemisorption reaction without a transition state and does not require ΔE,

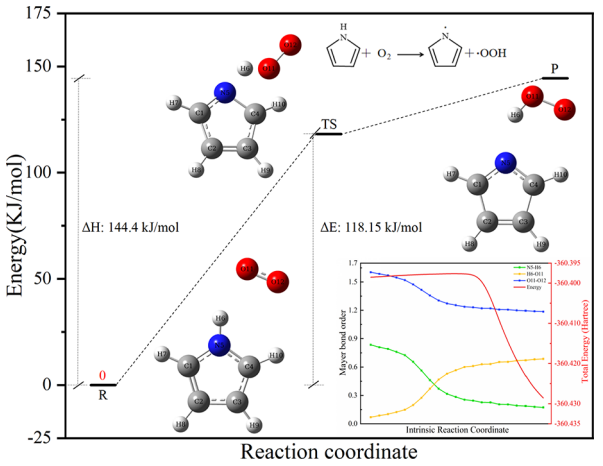

Figure 3. Reaction potential energy diagram and Mayer bond order change (R2).

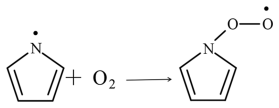

thereby releasing the energy of 31.51 kJ/mol to further promote the oxidation of coal.

3.2.2. Mechanism of the Reaction of Pyridine and Oxygen.

In the structure model of coal, the reaction equation of the oxidation of pyridine to the pyridinyl radical is shown in eq 4.

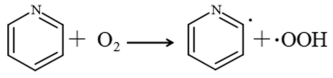

The energy barriers of the reactants, transition states, and products and, in the IRC pathway, the bond order changes of C5−H11, H11−O12, and O12−O13 are shown in Figure 4. First, the C5−H11 bond order gradually decreases during the oxygen capture of H11 in the pyridine structure, indicating that the C5−H11 bond is weakened and tends to break. The bond order of H11−O12 gradually increases along the IRC curve. The broken H11 interacts with O12−O13 to form ·OOH and a pyridinyl radical. The bond length R(C5,H11) extends from 1.08 to 1.51 Å and R(O12,H11) shortens from 2.69 to 1.07 Å during the abstraction of an H atom on C5 at the pyridine neighboring site by oxygen. The reaction needs to overcome the energy barrier of 86.642 kJ/mol and absorb 112.897 kJ/mol of heat. Therefore, the reaction cannot occur spontaneously at room temperature. The pyridinyl radical recombines

https://doi.org/10.1021/acsomega.3c05088
ACS Omega 2023, 8, 35295−35306

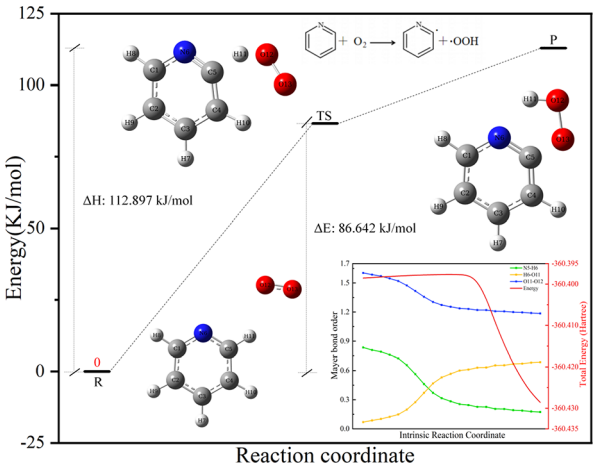

Figure 4. Reaction potential energy diagram and Mayer bond order change (R4).

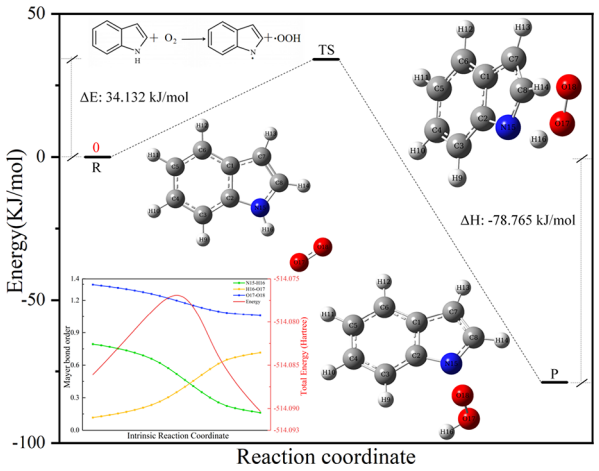

Figure 5. Reaction potential energy diagram and Mayer bond order change (R6).

with oxygen to form pyridinyl peroxy radical intermediates with the reaction equation shown in eq 5. The reaction does

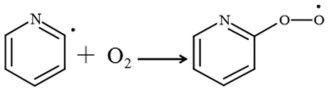

not need to cross the energy barrier and releases 16.089 kJ/mol of heat. As the reaction proceeds, the pyridinyl peroxyl radical intermediate is further decomposed to produce HCN and NH_3.

3.2.3. Mechanism of the Reaction of Indole and Oxygen.

Indole, as a nitrogen containing five-membered heterocyclic structure,[36,37] undergoes a two-step oxidation pathway. Initially, the N−H bond within the indole structure breaks upon the attack of O_2, thereby resulting in the generation of an indolyl radical and H_2O, as shown in eq 6. Subsequently, the

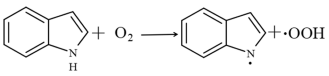

indolyl radical undergoes further oxidation, leading to the formation of an indolyl peroxyl radical, as shown in eq 7.

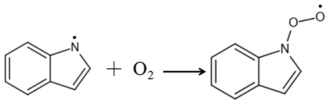

Figure 5 illustrates the energy barrier change and the Mayer bond order change along the IRC curve for the reaction transition state of eq 6. Along the IRC curve, the bond order of the N15−H16 bond gradually weakens, while the atomic spacing between H16 and O17 gradually decreases and the bond order gradually increases. As the reaction progresses, the bond order of the O17−O18 bond weakens and combines with H16 to form ·OOH. Meanwhile, the bond length R(N15,H16) increases from 1.01 to 1.22 Å and R(O17,H16) decreases from 2.00 to 1.32 Å. Moreover, N15, O17, and H16 a bond angle of 134.17°. The reaction needs to overcome an energy barrier of 34.132 kJ/mol and release heat of 78.765 kJ/mol. Therefore, the reaction can proceed spontaneously at room temperature. The indolyl radical, generated through the oxidation of indole, reacts with oxygen again to form an indolyl peroxy radical. This reaction occurs without the need to cross a barrier and releases 23.934 kJ/mol of heat.

3.2.4. Mechanism of the Reaction of Quinoline and Oxygen.

The oxidation reaction of quinoline is represented by eq 8. This reaction is mainly manifested as the loss of an H atom

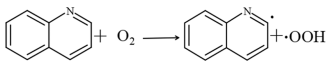

from the N-linked carbon in the quinoline structure, which then combines with oxygen to generate a quinolinyl radical and ·OOH. As shown in Figure 6, the bond orders of O18−O19

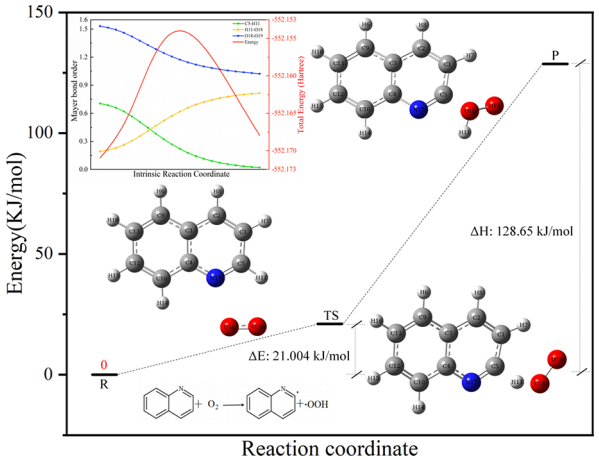

Figure 6. Reaction potential energy diagram and Mayer bond order change (R8).

and C5−H11 atoms gradually decrease and the distance between O18 and H11 atoms in the O18−O19 bond approaches, resulting in the formation of ·OOH. The reaction path is summarized as the dehydrogenation of quinoline with O_2, the fission of the C5−H11 bond, and the bimolecular reaction of H11 with O18−O19 to form a quinolinyl radical and ·OOH. The reaction needs to overcome the energy barrier of 34.132 kJ/mol and absorb the heat of 78.765 kJ/mol so it can spontaneously occur at room temperature.

3.2.5. Mechanism of the Reaction of Carbazole and Oxygen.

https://doi.org/10.1021/acsomega.3c05088
ACS Omega 2023, 8, 35295−35306

Carbazole is less aromatic than pyrrole,[38] and its oxidation reaction is shown in eq 9. O_2 attacks N21−H22 bond in

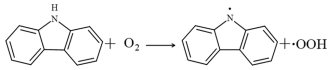

carbazole and absorbs the H atom to form a carbazolyl radical and ·OOH. The bond order of N21−H22 decreases with IRC until fracture occurs. The bond order of H22−O23 gradually increases with decreasing IRC and the bond order of O23−O24 gradually decreases. The broken H22 combines with O23−O24. The reaction needs to overcome the 47.259 kJ/mol energy barrier and releases 81.391 kJ/mol of energy, as shown in Figure 7. The oxidation of carbazole can occur exothermically in an environment below 70 °C.

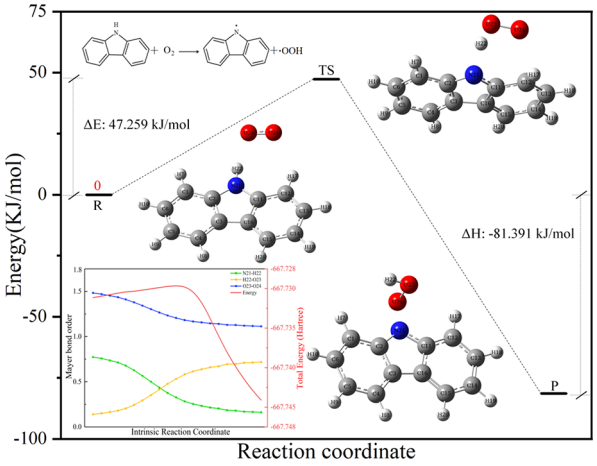

Figure 7. Reaction potential energy diagram and Mayer bond order change (R9).

3.3. Reaction mechanism of ·OH scavenging by NCOSs. Figure 8 depicts the reaction pathway for the extraction of H to produce H_2O from NCOSs by ·OH. Figure 9 displays the Mayer bond order changes along the IRC curve for each reaction transition state. ·OH extracts the H atom from pyrrole to produce an unstable five-membered nitrogenous structure with a lone pair electron-pyrrolyl radical and H_2O (R10). The IRI equivalent surface can show the bonding changes of atoms at IRC representative points during the reaction. Figure 10 displays the pyrrole structure at various points and the changes in the bond length of N5−H6 and H6−O11 on the IRC path of the reaction transition state in the presence of ·OH. The last point of the path corresponds to the reactants pyrrole and ·OH. Throughout the chemical process, that is, from the reactant to TS, the bond length R(N5,H6) increases from 1.04 to 1.14 Å, N5−H6 gradually breaks, and H6−O11 to be formed strengthens with a change in bond length R from 1.63 to 1.37 Å. After passing TS, the IRI equivalent surface of newly generated H6−O11 elongates along the bonding direction, suggesting that the bond approaches the ordinary H−O bond, at which time N5−H6 increases to the bond length of 1.56 Å and H6−O11 decreases to 0.98 Å. Finally, H_2O and the pyrrolyl radical, which fully show the change in atomic bonding, are formed. According to eq 11, ·OH abstracts H11 from C5 in pyridine, resulting in the formation of a pyridinyl radical and H_2O. During the reaction, the bond order of C5−H11 decreases from 0.78 to 0.14, which leads to the weakening of the bond binding force; the bond energy of H11−O12 increases from 0.14 to 0.75, and the H atom interacts with ·OH to form H_2O and a pyridinyl radical. Figure 11 shows the change of the bond length along the IRC path of the reaction transition state of eq 11. C5−H11 breaks preferentially and gradually transitions to H11−O12, the bond length R(C5,H11) increases from 1.12 to 1.21 Å, and the bond length R(H11,O12) decreases from 1.57 to 1.31 Å, resulting in a transition state. The formation of the pyridinyl radical and H_2O is promoted until the bond lengths of C5−H11 and H11−O12 reach 1.67 and 1.08 Å, respectively.

The reactions of ·OH capturing H atoms in indole and carbazole are expressed in eqs 12 and 13, respectively. Indole reacts with ·OH to form an indolyl radical and H_2O; carbazole interacts with ·OH to form a carbazolyl radical and H_2O. The bond order of N15−H16 gradually weakens from 0.8 to 0.14 along the reaction path, and the bond order of H16−O17 increases from 0.12 to 0.75, that is, H16 approaches ·OH and eventually combines to form H_2O. The bond order of N21−H22 in carbazole decreases from 0.77 to 0.16 along the IRC curve, and the bond order of H22−O23 increases from 0.14 to 0.72, and the H broken in N21−H22 forms H_2O and carbazolyl radical with ·OH. Equation 14 corresponds to the reaction in which ·OH captures the H atom on quinoline C5−H11 to form a quinolinyl radical and H_2O. The bond order between C5−H11 weakens from 0.79 to 0.13, and the bond order between H11 and O18 increases from 0.14 to 0.76, thereby promoting the formation of H_2O. In summary, ·OH consumes NCOSs and also reduces the amount of ·OH during low-temperature oxidation. This finding is in agreement with the results obtained by Wu et al.[25]

3.4. Circular Chain Pathways of NCOSs. Figure 12 depicts the reaction pathways of NCOSs during coal oxidation.

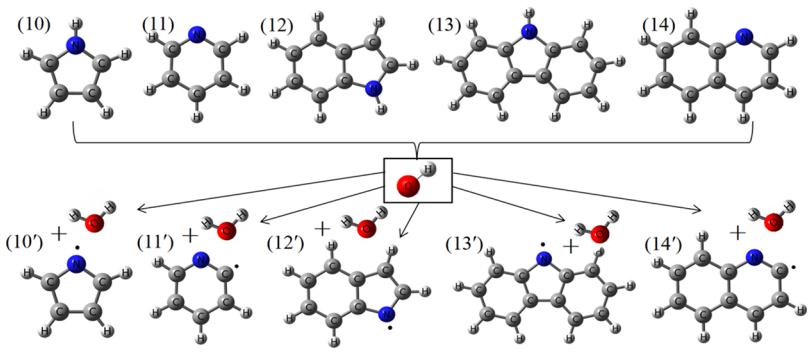

Figure 8. Mechanism of the reaction between NCOSs and ·OH.

https://doi.org/10.1021/acsomega.3c05088
ACS Omega 2023, 8, 35295−35306

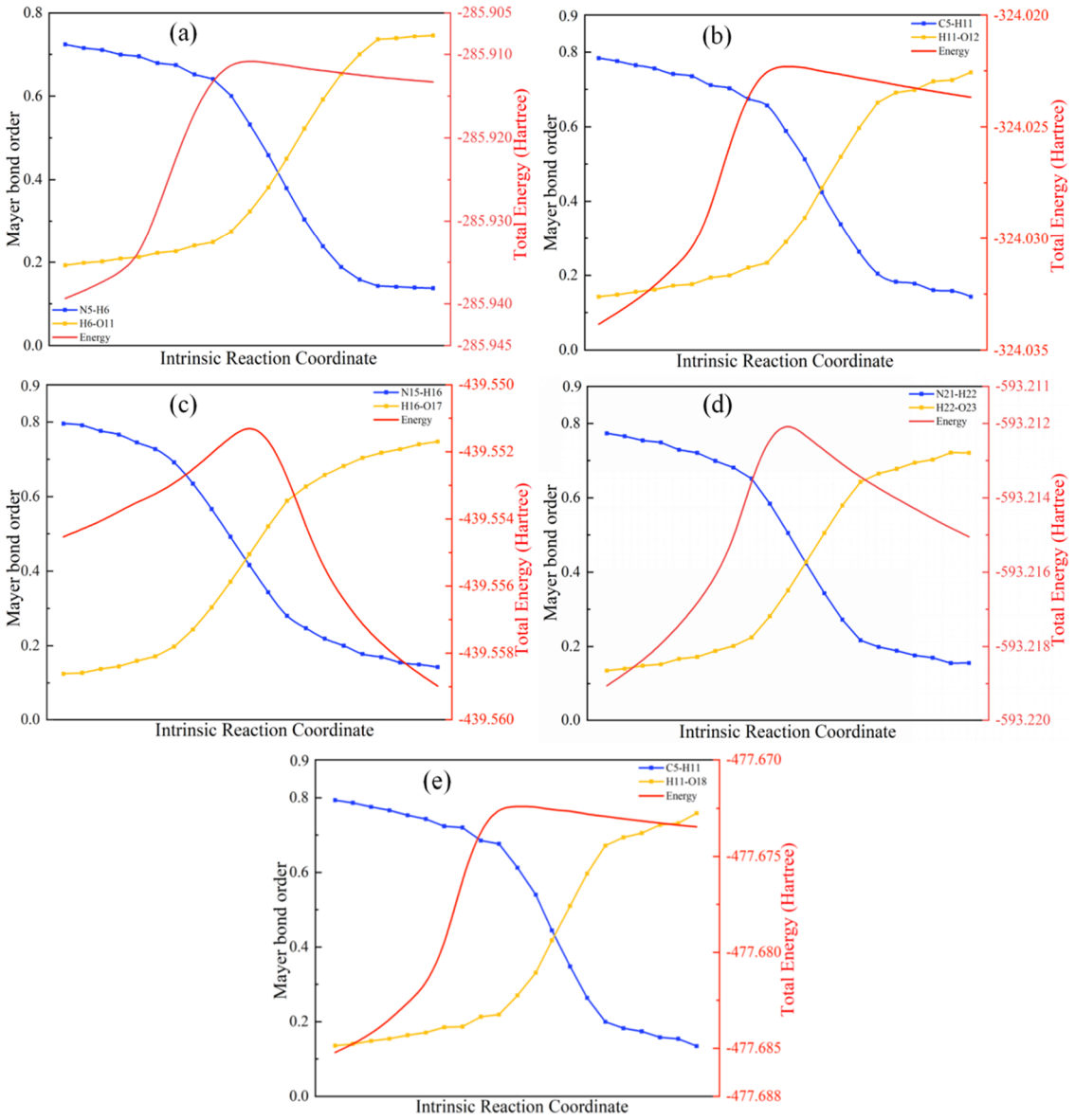

Figure 9. Mayer bond orders along the IRC of transition: (a) R10; (b) R11; (c) R12; (d) R13; (e) R14.

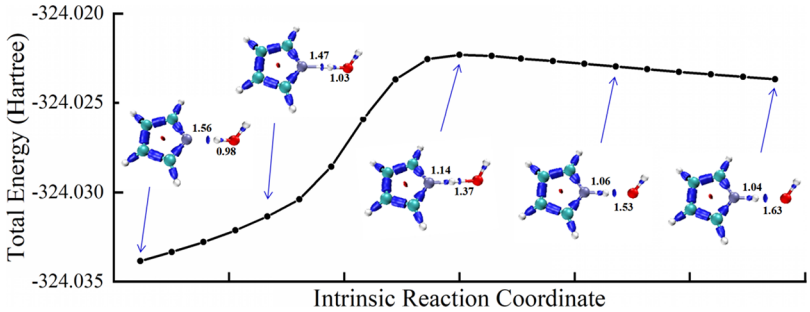

Figure 10. IRI equivalent surface of IRC representative points (R10).

Depending on the difference between N-5 and N-6 during coal oxidation, the process involves the breakage of N−H and C−H bonds and the formation of nitrogenous radicals and ·OOH. The resulting pyrrolyl and pyridinyl radicals adsorb O_2 undergo addition reactions to peroxide radicals (ROO·). The reaction does not require overcoming energy barriers and occurs at room temperature. ROO· captures H atoms from adjacent carbon groups to form a carbon radical (R·) and hydroperoxide products. The decomposition of hydroperoxide is the main reaction pathway for ·OH formation. At an energy barrier of 317.69 kJ/mol, the O−O bond of ·OOH breaks to produce ·OH.[14] ·OH plays a role in chain reaction. It consumes the active sites in the coal structure and abstracts the H atoms of NCOSs in coal to generate nitrogen radicals

https://doi.org/10.1021/acsomega.3c05088
ACS Omega 2023, 8, 35295−35306

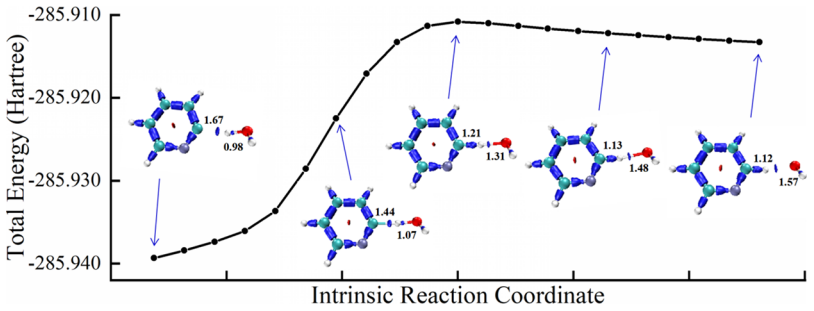

Figure 11. IRI equivalent surface of IRC representative points (R11).

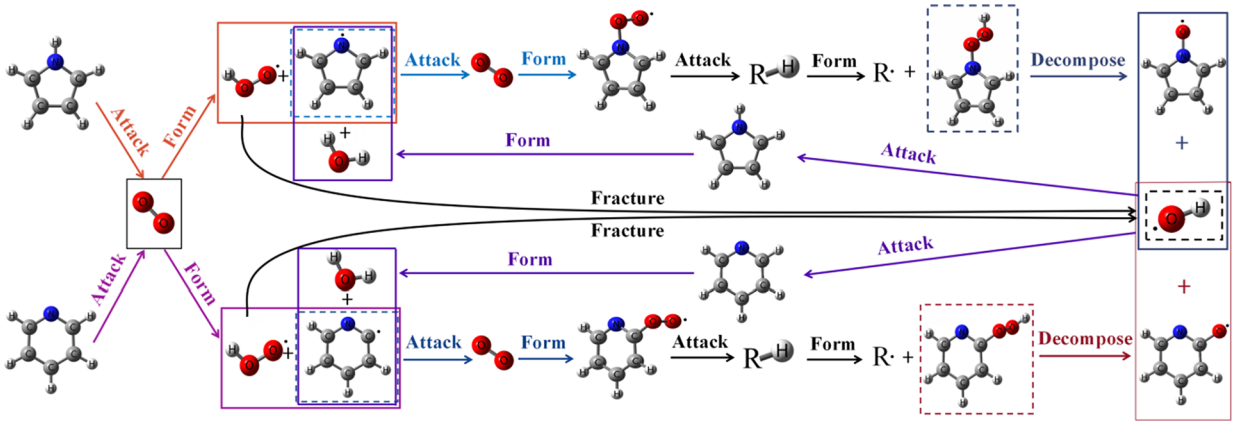

Figure 12. Reaction pathway and cycle model of NCOSs in the CSC process.

and H_2O. The reactive nitrogen radicals generated during this reaction continue to interact with oxygen to form ROO·, thereby prompting subsequent reactions to occur one after another. As the reaction continues, a cyclic chain reaction is eventually formed. The presence of ROO· and ·OH drives the chain reaction. Therefore, the presence of ROO· and ·OH must be prevented to inhibit CSC.

3.5. Thermodynamic Characterization of NCOSs.

Figure 13 illustrates the changes in the free energy of pyrrole, pyridine, indole, quinoline, and carbazole under attack by oxygen and ·OH. The ΔE value for the reaction of H on NCOSs trapped by ·OH is lower than 30 kJ/mol and can react spontaneously at room temperature. Among them, pyrrole, pyridine, carbazole, indole, and quinoline exhibit varying levels of ease in undergoing reaction. The activation energies of these compounds are 28.88, 21.004, 23.63, 18.379, and 18.379 kJ/mol, respectively. However, the ΔE value for O_2 capture of H on NCOSs is relatively high; the ΔE of O_2 attacking H in the pyrrole structure is 118.15 kJ/mol, and the reaction temperature needs to be in the range of 70−200 °C. Attacking H of the carbazole and pyridine structures needs to overcome energy of 47.259 and 86.642 kJ/mol, respectively, and the reaction can occur at temperatures below 70 °C; the ΔE for attacking H in indole and quinoline is 34.132 and 20.004 kJ/mol, respectively, and can react spontaneously at room temperature. Therefore, O_2 has the strongest ability to capture H in quinoline, and the ability to capture H in NCOSs from strong to weak is quinoline, indole, pyridine, pyrrole, and carbazole, in order. Figure 14 shows the changes in the enthalpy of oxygen and the ·OH attack on NCOSs. The reactions of ·OH capturing H in pyrrole, pyridine, indole, quinoline, and carbazole all exhibit exothermic reactions with heat releases of 49.89, 7.877, 123.399, 13.128, and 115.522 kJ/mol, respectively. Among them, indole releases the most heat when a reaction occurs. The changes in the enthalpy of O_2 trapping H in pyrrole, pyridine, indole, quinolone, and carbazole are 144.4, 112.897, 78.765, 128.65, and 81.391 kJ/mol, respectively, and O_2 capturing H in pyrrole absorbs the most heat at 144.4 kJ/mol. Hence, its contribution to the oxidation process of coal does not contribute to the increase in temperature.

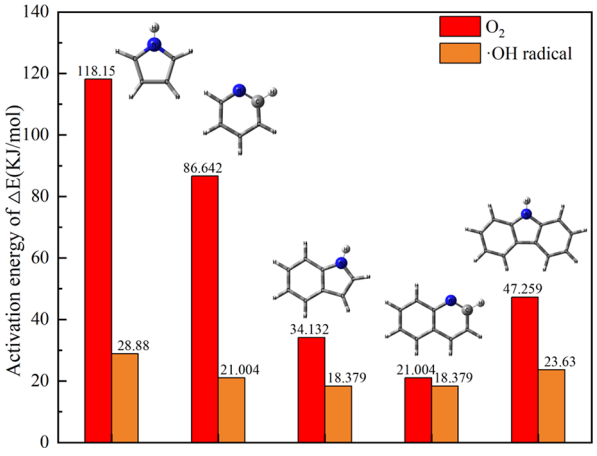

Figure 13. Oxidation and ·OH path with NCOSs of free energy change.

Figure 15 shows the characteristics of the reaction rate changes when NCOSs are attacked by oxygen and ·OH in the interval of 25 to 200 °C. At the same temperature, ·OH captures H atoms in pyrrole, pyridine, indole, quinoline, and carbazole at the corresponding rate constants of 3.68×10^{-32},

https://doi.org/10.1021/acsomega.3c05088
ACS Omega 2023, 8, 35295−35306

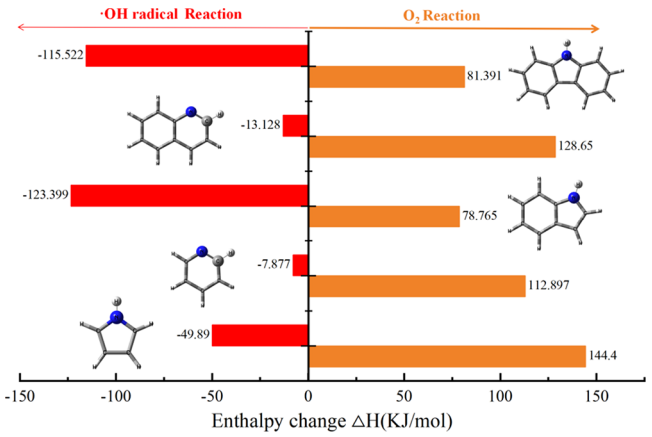

Figure 14. Oxidation and ·OH path with NCOSs of enthalpy change free energy change.

1.05×10^{-32}, 1.62×10^{-16}, 2.84×10^{-27}, and 6.70×10^{-18} $cm^3/mol/s$; O_2 hydrogen trapping reactions correspond to K^{TST} of 2.22×10^{-12}, 5.35×10^{-11}, 7.75×10^{-13}, 1.53×10^{-10}, and 1.88×10^{-11} $cm^3/mol/s$, respectively. The maximum k^{TST} of the quinoline oxidation process is 1.53×10^{-10} $cm^3/mol/s$; the rate constant of capturing H atoms in indole by ·OH is 1.62×10^{-16} $cm^3/mol/s$. Therefore, the reaction rate constant for capturing H atoms in NCOSs by O_2 is much higher than that for capturing H by ·OH. As the temperature increases, the reaction rate constant of the oxidation process increases, leading to the rapid onset of the coal reaction and a further increase in the oxygen consumption rate.

3.6. XPS Experimental Analysis. Figures 16 and 17 17show the peak-fitted N1spectra of HM, JM, FM, CY, and WY coal samples at room temperature, 70, and 200 °C. The spectra can be fitted with four peaks that correspond to pyridinic N (N-6) at 398.4 ± 0.2 eV, pyrrolic N (N-5) at 400.3 ± 0.2 eV, quaternary N (N-Q) at 401.4 ± 0.2 eV, and oxidized N (N-X) at 403.2 ± 0.2 eV.[39] The nitrogen in coal was mainly found to be in the of N-5 and N-6, both with a relatively large share of the peak area. A small amount of N-Q and N-X within the large aromatic structure (≥5 rings) can also be observed. Table 3 presents the distribution of peak areas for each nitrogen relative to the total peak areas of N 1s in the coal samples. Notably, the contents of the N-5 and N-6 structures are prominently dominant. At room temperature, the contents of HM, CY, FM, JM, and WY were 41.51% and 31.61%, 40.97% and 34.5%, 38.05% and 35.11%, 36.03% and 36.48%, and 35.1% and 37.63%, respectively. Upon analysis of the five coal samples, the N-6 content increases while the N-5 content decreases on the coal surface, indicating an increase in aromaticity. However, N-Q and N-X s in NCOSs are present in lesser amounts. Their content does not change significantly with increasing coalification; that is, they are less influenced by coalification. The proportion of nitrogen forms on the coal surface changed with increasing coal oxidation temperature, and N-5 and N-6 predominate over other nitrogen forms at all temperatures.

The N 1s spectra of HM, CY, FM, JM, and WY at oxidation conditions of 70 and 200 °C are shown in Figure 17a,b, respectively. The proportion of N-5 content in coal decreases; at 70 °C, going from 41.51, 40.97, 38.05, 36.03, and 35.1% to 39.99, 38.23, 37.4, 29.48, and 28.93%; at 200 °C, it decreases to 38.65, 38.18, 36.03, 35.03, and 33.26%, respectively. This reduction is primarily attributed to the reaction of carbazole, which overcomes an energy barrier of 47.259 kJ/mol during coal oxidation up to 70 °C. As the temperature increases to 70−200 °C, pyrrole undergoes oxidation to overcome the 118.5 kJ/mol energy barrier. The proportion of N-6 content at 70 °C shows a decreasing trend and decreases from 31.61, 34.5, 35.11, 36.48, and 37.63% to 28.41, 29.89, 30.96, 30.93, and 31.68%, mainly because of the oxidation reaction of pyridine across 86.642 kJ/mol under an environment below 70 °C; at 200 °C are 33.2, 33.35, 34.75, 34.18, and 34.44% in

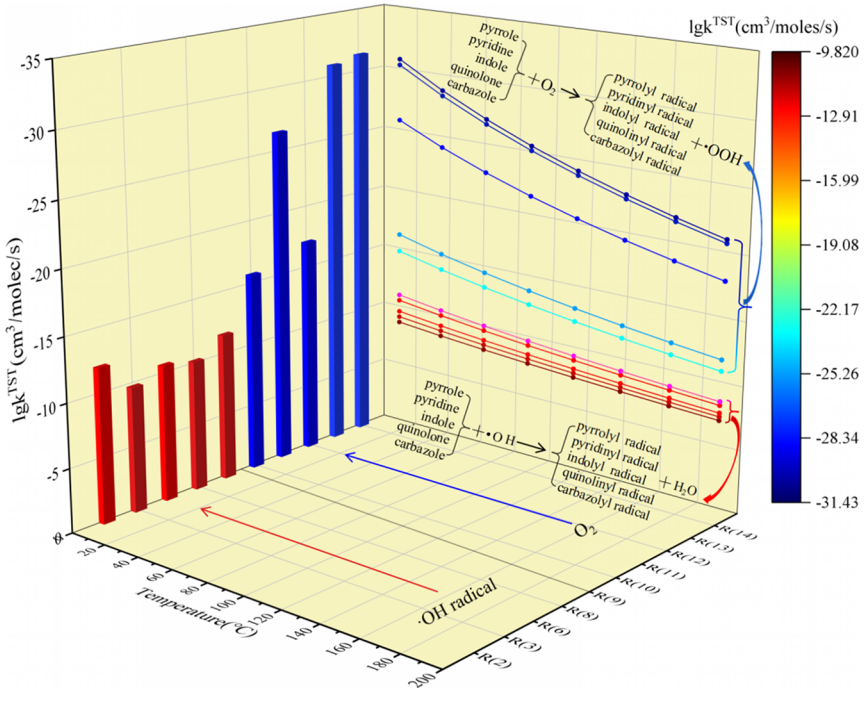

Figure 15. Reaction rates of NCOSs between 25 and 200 °C.

https://doi.org/10.1021/acsomega.3c05088
ACS Omega 2023, 8, 35295−35306

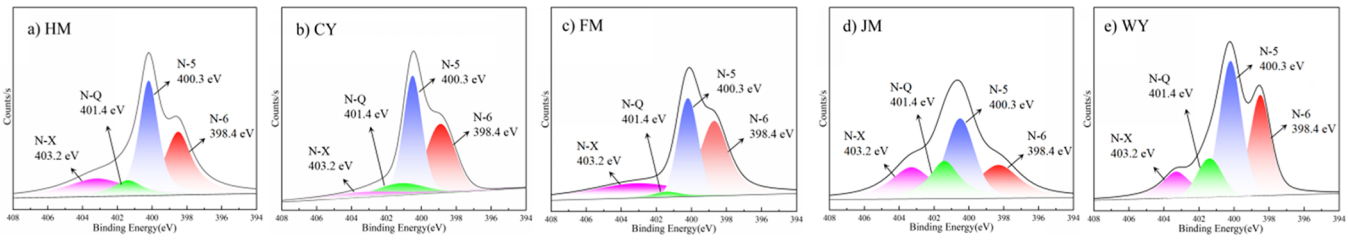

Figure 16. N 1s peak fitting of coal samples at room temperature.

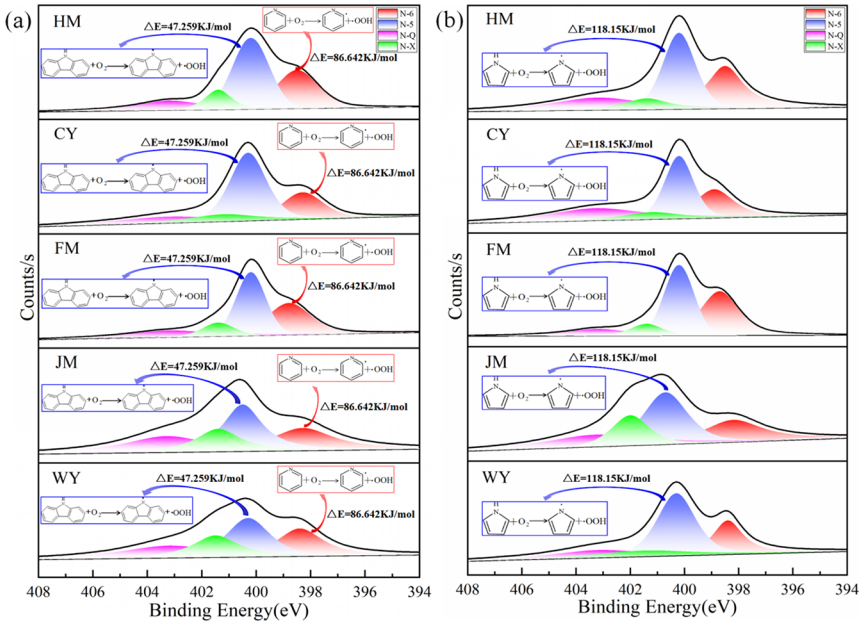

Figure 17. N 1s spectrum of oxidation heating process: (a) 70 °C; (b) 200 °C.

Table 3. Relative Percentage Content of Specific Functional Groups of Coal Samples at Room Temperature and Oxidation Temperature (%)

coals	T/°C	N-5 (%)	N-6 (%)	N-Q (%)	N-X (%)
HM	30	41.51	31.61	8.63	18.25
	70	39.99	28.41	13.35	18.25
	200	38.65	33.2	7.92	20.23
CY	30	40.97	34.5	10.15	14.38
	70	38.23	29.89	13.1	18.78
	200	38.18	33.35	8.32	20.15
FM	30	38.05	35.11	4.79	22.05
	70	37.4	30.96	13.29	18.35
	200	36.03	34.75	11.16	18.06
JM	30	36.03	36.48	13.06	14.43
	70	29.48	30.93	17.12	22.47
	200	35.03	34.18	16.03	14.76
WY	30	35.1	37.63	12.45	14.82
	70	28.93	31.68	17.81	21.58
	200	33.26	34.44	14.93	18.37

order and do not vary significantly. The proportions of N-Q and N-X content during the oxidation process are relatively small and exhibit minimal changes. Hence, they are not discussed here. The analytical results indicate that the content proportions of NCOSs vary with the oxidation temperature. Reactions that cross the energy barrier of 40−100 kJ/mol occur at 30−70 °C, leading to a decrease in the content proportion of carbazole and pyridine. A reaction that crosses an energy barrier higher than 100 kJ/mol occurs at 70−200 °C, resulting in a significant decrease in the content proportion of pyrrole. Therefore, the XPS spectra of nitrogen on the coal surface are compared at different temperatures to further confirm the NCOSs before and after coal oxidation. This result also demonstrates the relationship between the reaction energy barrier and temperature in the oxidation process of NCOSs, which is consistent with the discussion results of this issue in Section 3.5. Therefore, the ΔE barrier can be used as an indicator of the overall oxidation change in the temperature range discussed.

4. CONCLUSIONS

Pyrrole, pyridine, indole, quinoline, and carbazole interact with O_2 to generate ·OOH and radicals such as pyrrolyl, pyridinyl, indolyl, quinolinyl, and carbazolyl. Subsequently, the nitrogenous radicals spontaneously adsorb O_2 to ROO· and release heat. ROO· undergoes self-reaction; the O−O bond breaks and dehydrogenates to ·OH; the O−O bond breaks on ·OOH to ·OH. Then, the reaction of ·OH with pyrrole, pyridine, indole, quinoline, and carbazole at room temperature generates H_2O and radicals such as pyrrolyl, pyridinyl, indolyl, quinolinyl, and carbazolyl, respectively, thus forming a cyclic chain reaction.

During the low-temperature oxidation of coal, indole and quinoline require 34.132 and 21.004 kJ/mol of energy to be oxidized, respectively. Thus, the reaction

https://doi.org/10.1021/acsomega.3c05088
ACS Omega 2023, 8, 35295−35306

proceeds spontaneously at room temperature. Carbazole and pyridine need to overcome 47.259 and 86.642 kJ/mol of energy barriers to be attacked by oxygen, respectively, so the N-5 and N-6 contents decrease significantly when the temperature rises to 70 °C. The oxidation of pyrrole needs to cross an 118.5 kJ/mol energy barrier, so the N-5 content decreases significantly when the temperature rises to 200 °C. The H atoms in pyrrole, pyridine, indole, quinoline, and carbazole were captured by ·OH, corresponding to the activation energies of 28.88, 21.004, 18.379, 18.379, and 23.63 kJ/mol, respectively. Thus, reactions can proceed spontaneously at room temperature with a low energy barrier and high exothermic characteristics.

AUTHOR INFORMATION

Corresponding Author

Zhilin Xi − *School of Environmental Science and Safety Engineering, Tianjin University of Technology, Tianjin 300384, China; Tianjin Key Laboratory of Hazardous Waste Safety Disposal and Recycling Technology, Tianjin 300384, China;* orcid.org/0000-0002-2058-9161; Phone: +86 22 60214184; Email: xzlsafety@tjut.edu.cn; Fax: +86 22 60214184

Authors

Mengmeng Zhang − *School of Environmental Science and Safety Engineering, Tianjin University of Technology, Tianjin 300384, China; Tianjin Key Laboratory of Hazardous Waste Safety Disposal and Recycling Technology, Tianjin 300384, China*

Zhensen Gong − *School of Environmental Science and Safety Engineering, Tianjin University of Technology, Tianjin 300384, China; Tianjin Key Laboratory of Hazardous Waste Safety Disposal and Recycling Technology, Tianjin 300384, China*

Yubo Dong − *School of Environmental Science and Safety Engineering, Tianjin University of Technology, Tianjin 300384, China; Tianjin Key Laboratory of Hazardous Waste Safety Disposal and Recycling Technology, Tianjin 300384, China*

Complete contact information is available at: https://pubs.acs.org/10.1021/acsomega.3c05088

Notes

The authors declare no competing financial interest.

ACKNOWLEDGMENTS

This work was supported partly by the "National Natural Science Funds of China (Grant Nos. 52274223 and 52074192)", partly by the "Tianjin Science and Technology Plan Major Special Project (Grant No. 18ZXAQSF00020)", partly by the "The general project of Tianjin Natural Science Founds (Grant No. 19JCYBJC23000)", and partly by the "Tianjin University of Technology Graduate Research Innovation Practice Project (Grant No. YJ2259)".

REFERENCES

(1) Wang, C. H.; Cheng, Y. P. Role of coal deformation energy in coal and gas outburst: A review. *Fuel* **2023**, *332*, No. 126019.

(2) NBS. Statistical Bulletin on National Economic and Social Development of the People's Republic of China, 2022.

(3) Xi, Z. L.; Wang, X. D.; Wang, X. L.; Wang, L.; Li, D.; Guo, X. Y.; Jin, L. W. Polymorphic foam clay for inhibiting the spontaneous combustion of coal. *Process Saf. Environ. Prot.* **2019**, *122*, 263−270.

(4) Belviso, C. State-of-the-art applications of fly ash from coal and biomass: A focus on zeolite synthesis processes and issues. *Prog. Energy Combust. Sci.* **2018**, *65*, 109−135.

(5) Wang, D. M.; Shao, Z. L.; Zhu, Y. F. Several scientific issues in major coal mine thermodynamic disasters. *J. Coal* **2021**, *46*, 57−64.

(6) Zhou, X. Q.; Zhou, B. X.; Zhu, H. Q.; Chang, W. J.; Guo, D. Theoretical study of ignition temperature characteristics when gas is detonated by frictional sparks. *J. Hunan Univ. Sci. Technol.* **2004**, *19*, 1798.

(7) Qin, B. T.; Zhong, X. X.; Wang, D. M.; Xin, H. H.; Shi, Q. L. Research progress of coal spontaneous combustion process characteristics and prevention technology. *Coal Sci. Technol.* **2021**, *49*, 66−99.

(8) Wang, D. M.; Xin, H. H.; Qi, X. Y.; Dou, G. L.; Qi, G. S.; Ma, L. Y. Reaction pathway of coal oxidation at low temperatures: a model of cyclic chain reactions and kinetic characteristics. *Combust. Flame* **2016**, *163*, 447−460.

(9) Zhou, B. Z.; Yang, S. Q.; Wang, C. J.; Hu, X. C.; Cai, J. W.; Xu, Q.; Sang, N. W. The characterization of free radical reaction in coal low-temperature oxidation with different oxygen concentration. *Fuel* **2020**, *262*, No. 116524.

(10) Xu, Q.; Yang, S. Q.; Cai, J. W.; Zhou, B. Z.; Xin, Y. A. Risk forecasting for spontaneous combustion of coals at different ranks due to free radicals and functional groups reaction. *Process Saf. Environ. Prot.* **2018**, *118*, 195−202.

(11) Zhou, B. Z.; Yang, S. Q.; Jiang, X. Y.; Cai, J. W.; Xu, Q.; Song, W. X.; Zhou, Q. C. The reaction of free radicals and functional groups during coal oxidation at low temperature under different oxygen concentrations. *Process Saf. Environ. Prot.* **2021**, *150*, 148−156.

(12) Xin, H. H.; Wang, D. M.; Zhong, X. X.; Xu, T.; Li, W. G. Distribution characteristics of functional groups on the surface of lignite particles and quantum chemical analysis. *Spectrosc. Lab* **2012**, *29*, 690−693.

(13) Chen, L. Z.; Qi, X. Y.; Zhang, Y. B.; Xin, H. H.; Liang, Z. Q. Reaction activity and mechanism of R3-CH structure oxidation in coal self-heating. *Fuel* **2021**, *290*, No. 119797.

(14) Xi, Z. L.; Li, M. M.; Li, X.; Lu, L. P.; Wang, J. W. Reaction mechanisms involving the hydroxyl radical in the low-temperature oxidation of coal. *Fuel* **2022**, *314*, No. 122732.

(15) Qi, X. Y.; Xue, H. B.; Xin, H. H.; Bai, Z. M. Quantum chemistry calculation of reaction pathways of carboxyl groups during coal self-heating. *Can. J. Chem.* **2017**, *95*, 824−829.

(16) Xi, Z. L.; Xi, K.; Lu, L. P.; Zhang, M. M. Study on oxidation characteristics and conversion of sulfur-containing model compounds in coal. *Fuel* **2023**, *331*, No. 125756.

(17) Cao, J. P.; Zong, Z. M.; Zhao, X. Y.; Sun, L. B.; Lee, C. W.; Zhao, W.; Wei, X. Y. Identification of Sulfur and Nitrogen-containing Organic Species in the Extracts from Pocahontas No. 3 Coal. *Energy Sources, Part A* **2010**, *32*, 1086−1099.

(18) Ikeda, E.; Nicholls, P.; Mackie, J. C. A kinetic study of the oxidation of pyridine. *Proc. Combust. Inst.* **2000**, *28*, 1709−1716.

(19) Zheng, M.; Li, X. X.; Guo, L. Investigation of N behavior during coal pyrolysis and oxidation using ReaxFF molecular dynamics. *Fuel* **2018**, *233*, 867−876.

(20) Laskin, A.; Lifshitz, A. Isomerization and Decomposition of Indole. Experimental Results and Kinetic Modeling. *J. Phys. Chem. A* **1997**, *101*, 7787−7801.

(21) Wu, L. N.; Tian, Z. Y.; Wang, D.; Zheng, Z. H.; Jin, K. R.; Liu, B. Z.; Xie, C.; Xu, Q.; Wang, Z. D. Dinitriles and nitriles are common intermediates of pyrrole pyrolysis. *Combust. Flame* **2022**, *245*, No. 112358.

(22) Wang, C. G.; Du, Y. B.; Jin, X.; Che, D. F. Pyridine and pyrrole oxidation under oxy-fuel conditions. *Energy Sources, Part A* **2016**, *38*, 1556−7036.

(23) Luo, J. H.; Zou, C.; Lin, Q. J.; Xia, W. X.; Zou, H. R.; Wang, S. S. A shock tube and modeling study on the auto-ignition properties of

pyrrole in O_2/CO_2 atmosphere at elevated pressures. *Combust. Flame* **2021**, *230*, No. 111458.
(24) Mai, T. V. T.; Nguyen, H. T.; Huynh, L. K. Ab initio kinetic mechanism of OH-initiated atmospheric oxidation of pyrrole. *Chemosphere* **2021**, *263*, No. 127850.
(25) Wu, L. N.; Tian, Z. Y.; Wang, J. J.; Yu, D.; Liu, Y. X.; Tian, D. X.; Cao, C. C.; Zou, J. B.; Zhang, Y.; Yang, J. Z. Experimental and kinetic study on the low-temperature oxidation of pyridine as a representative of fuel-N compounds. *Combust. Flame* **2019**, *202*, 394−404.
(26) Yamamoto, T.; Kuwahara, T.; Nakaso, K.; Yamamoto, T. Kinetic study of fuel NO formation from pyrrole type nitrogen. *Fuel* **2012**, *93*, 213−220.
(27) Yue, S.; Wang, C. B.; Huang, Y. L.; Xu, Z. Y.; Xing, J. Y.; Anthony, E. J. The role of H_2O in structural nitrogen migration during coal devolatilization under oxy-steam combustion conditions. *Fuel Process. Technol.* **2022**, *225*, No. 107040.
(28) Martoprawiro, M.; Bacskay, G. B.; Mackie, J. C. Ab Initio Quantum Chemical and Kinetic Modeling Study of the Pyrolysis Kinetics of Pyrrole. *J. Phys. Chem. A* **1999**, *103*, 3923−3934.
(29) Higashio, Y.; Shoji, T. Heterocyclic compounds such as pyrrole, pyridines, pyrro-lidine, piperidine, indole, imidazol and pyrazines. *Appl. Catal., A* **2004**, *260*, 251−259.
(30) Rahman, Z. U.; Wang, X. B.; Zhang, J. Y.; Yang, Z. W.; Dai, G. F.; Verma, P.; Mikulcic, H.; Vujanovic, M.; Tan, H. Z.; Axelbaum, R. L. Nitrogen evolution, NOX formation and reduction in pressurized oxy coal combustion. *Renewable Sustainable Energy Rev.* **2022**, *157*, No. 112020.
(31) Fan, L. L.; Meng, X. L.; Zhao, J. Q.; Zhou, Y.; Chu, R. Z.; Yu, S.; Li, W. S.; Wu, G. G.; Jiang, X. F.; Miao, Z. Y. Reaction site evolution during low-temperature oxidation of low-rank coal. *Fuel* **2022**, *327*, No. 125195.
(32) Krishna, D. N. G.; Philip, J. Review on surface-characterization applications of X-ray photoelectron spectroscopy (XPS): Recent developments and challenges. *Appl. Surf. Sci. Adv.* **2022**, *12*, No. 100332.
(33) Lu, T.; Manzetti, S. Wave function and reactivity study of benzo[a]pyrene diol epoxide and its enantiomeric forms. *Struct. Chem.* **2014**, *25*, 1521−1533.
(34) Jiang, J. Y.; Zhang, S.; Longhurst, P.; Yang, W. H.; Zheng, S. J. Molecular structure characterization of bituminous coal in Northern China via XRD, Raman and FTIR spectroscopy. *Spectrochim. Acta, Part A* **2021**, *255*, No. 119724.
(35) Cai, S. S.; Zhang, S. F.; Wei, Y. Y.; Sher, F.; Wen, L. Y.; Xu, J.; Dang, J.; Hu, L. W. A novel method for removing organic sulfur from high-sulfur coal: Migration of organic sulfur during microwave treatment with NaOH-H_2O_2. *Fuel* **2021**, *289*, No. 119800.
(36) Liu, J.; Zhang, X. L.; Hu, B.; Lu, Q.; Liu, D. J.; Dong, C. Q.; Yang, Y. P. Formation mechanism of HCN and NH_3 during indole pyrolysis: A theoretical DFT study. *J. Energy Inst.* **2020**, *93*, 649−657.
(37) Zhou, X. F.; Liu, R. F. A density functional theory study of the pyrolysis mechanisms of indole. *J. Mol. Struct.: THEOCHEM* **1999**, *461*, 569−579.
(38) Alzueta, M. U.; Tena, A.; Bilbao, R. Pyridine conversion in a flow reactor and its interaction with nitric oxide. *Combust. Sci. Technol.* **2002**, *174*, 151−169.
(39) Ahmadi, S.; Khemiri, N.; Cantarero, A.; Kanzari, M. XPS analysis and structural characterization of CZTS thin films deposited by one-step thermal evaporation. *J. Alloys Compd.* **2022**, *925*, No. 166520.

https://doi.org/10.1021/acsomega.3c05088
ACS Omega 2023, 8, 35295−35306